Communication

Far-Red Photoactivatable BODIPYs for the Super-Resolution Imaging of Live Cells

YANG ZHANG, Ki-Hee Song, Sicheng Tang, Laura Ravelo, Janet Cusido, Cheng Sun, Hao F. Zhang, and Françisco M. Raymo

J. Am. Chem. Soc., **Just Accepted Manuscript** • DOI: 10.1021/jacs.8b09099 • Publication Date (Web): 24 Sep 2018

Far-Red Photoactivatable BODIPYs for the Super-Resolution Imaging of Live Cells

Yang Zhang,[†,§] Ki-Hee Song,[§] Sicheng Tang,[†] Laura Ravelo,[†] Janet Cusido,[†,‡] Cheng Sun,[¶] Hao F. Zhang[§,*] and Françisco M. Raymo[†,*]

[†]Laboratory for Molecular Photonics, Department of Chemistry, University of Miami, 1301 Memorial Drive, Coral Gables, FL 33146-0431, [‡]Department of Natural and Social Sciences, Miami Dade College – InterAmerican Campus, 627 S.W. 27th Avenue, Miami, FL 33135-2937 and Departments of [§]Biomedical Engineering and [¶]Mechanical Engineering, Northwestern University, 2145 Sheridan Road, Evanston, IL 60208

Supporting Information

ABSTRACT: The photoinduced disconnection of an oxazine heterocycle from a borondipyrromethene (BODIPY) chromophore activates bright far-red fluorescence. The high brightness of the product and the lack of autofluorescence in this spectral region allow its detection at the single-molecule level within the organelles of live cells. Indeed, these photoactivatable fluorophores localize in lysosomal compartments and remain covalently immobilized within these organelles. The suppression of diffusion allows the reiterative reconstruction of sub-diffraction images and the visualization of the labeled organelles with excellent localization precision. Thus, the combination of photochemical, photophysical and structural properties designed into our fluorophores enable the visualization of live cells with a spatial resolution that is inaccessible to conventional fluorescence imaging.

The advent of super-resolution imaging[1–3] is stimulating the design of fluorescent probes with appropriate properties for the sub-diffraction visualization of biological specimens. Most of the synthetic dyes developed for these applications are cyanine and xanthene derivatives with a few notable exceptions.[4–7] Despite their synthetic versatility and outstanding properties,[8–15] BODIPY chromophores have not been explored in this context, apart from two remarkable examples.[16,17] Both are based on photoswitching and detection of BODIPY fluorescence at the single-molecule level. In fact, structural designs to photoactivate BODIPY emission have actually been reported in the literature already.[18–22] Most of them are based on the photoinduced disconnection of a quencher from a BODIPY chromophore with concomitant fluorescence enhancement. In principle, these compounds could be exploited to reconstruct sub-diffraction images by photoactivated localization microscopy (PALM).[23,24] However, the modest fluorescence contrast accessible with these switching mechanisms complicate detection at the single-molecule level. Additionally, the initial and final states of these systems generally absorb in the same spectral window, preventing the selective photobleaching of the latter in the presence of the former necessary for the sequential reconstruction of PALM images.

Our laboratories devised a photochemical mechanism to shift bathochromically the main absorption of a BODIPY chromophore and allow the selective excitation of the product.[25–29] The overall result is fluorescence activation with infinite contrast and the spectral resolution of the absorptions of initial and final states. This behavior suggests that photoactivable BODIPYs with optimal properties for the implementation of PALM schemes can be developed relying on these photochemical transformations. This article reports the chemical synthesis and spectroscopic characterization of members of this family of photoactivatable fluorophores specifically designed for PALM and their ability to enable the sub-diffraction visualization of intracellular compartments in live cells.

A BODIPY fluorophore is connected to a photoswitchable auxochrome and a styryl appendage within **1** and **3** (Figure 1). Both molecules were synthesized in two steps from known precursors (Figure S1). They differ in the nature of the group (R^2) on position 4 of the styryl substituent, which is a hydrogen atom in **1** and a methoxy group in **3**. The corresponding absorption spectra (***a*** in Figures 2 and S3) show the characteristic BODIPY band with a maximum at a wavelength (λ_{Ab} in Table S1) of 609 nm for **1** and 618 nm for **3** in tetrahydrofuran (THF) and a molar absorption coefficient (ε) of 73.0 and 87.6 mM^{-1} cm^{-1} respectively. The emission spectra (***c*** in Figures 2 and S3) also show the characteristic BODIPY band with a maximum at a wavelength (λ_{Em}) of 624 nm for **1** and 635 nm for **3** and a fluorescence quantum yield (ϕ_F) of 0.85 and 0.80 respectively. These relatively high ε and ϕ_F values correspond to a brightness ($\varepsilon \times \phi_F$) of 62 mM^{-1} cm^{-1} for **1** and 66 mM^{-1} cm^{-1} for **3**.

Illumination of THF solutions of **1** and **3** at a λ_{Ac} in the spectral region where their *ortho*-nitrobenzyl fragment absorbs cleaves irreversibly the oxazine heterocycle to produce **2** and **4** respectively and release **7**. This photoinduced transformation

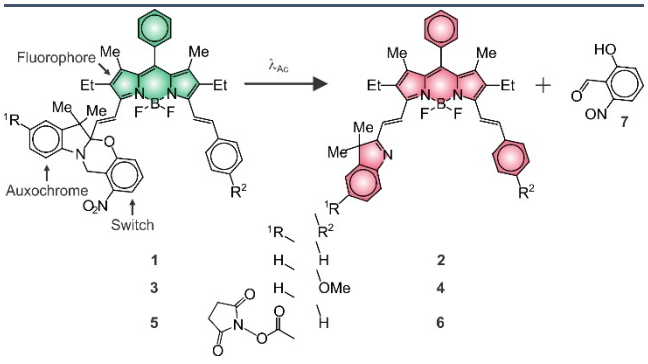

Figure 1. Photoinduced conversion of **1**, **3** and **5** into **2**, **4** and **6**.

converts the chiral center of the reactant into a sp^2 carbon atom in the product and brings the BODIPY chromophore in electronic conjugation with the indole auxochrome. As a result, the BODIPY absorption shifts bathochromically (***b*** in Figures 2 and S3) to a λ_{Ab} of 653 nm for **2** and 664 nm for **4** with ε of 72.8 and 86.7 mM^{-1} cm^{-1} respectively. Indeed, absorption spectra (***e*** in Figures 2 and S5) of THF solutions of **1** and **3**, recorded over the course of the photolytic transformation, show the developing absorption of the photochemical product in both instances. Analysis of the temporal absorbance evolution indicates the quantum yield for the photochemical formation of **2** and **4** to be 0.02 and 0.04 respectively. Furthermore, the pronounced bathochromic shift in absorption associated with the photoinduced conversion of **1** into **3** and of **2** into **4** allows the selective excitation of the photochemical product with concomitant fluorescence. Specifically, **2** emits at a λ_{Em} of 666 nm with a ϕ_F of 0.41 and a $\varepsilon \times \phi_F$ of 30 mM^{-1} cm^{-1} and **4** produces fluorescence at a λ_{Em} of 679 nm with a ϕ_F of 0.23 and a $\varepsilon \times \phi_F$ of 20 mM^{-1} cm^{-1}.

The depressive effect of the methoxy group on the ϕ_F of the photochemical product suggested the structural modification of the unsubstituted system only to permit bioconjugation. In particular, an active ester (R^1) was introduced in position 5 of the indole heterocycle of **1** to generate **5**. This molecule was prepared in two synthetic steps from known precursors (Figure S2). Its absorption and emission spectra (***a*** and ***c*** in Figure S9) show the active ester to have negligible influence on the position of the BODIPY bands, in agreement with the fact that the photocleavable auxochrome and fluorescent chromophore are isolated electronically in the ground state. Indeed, λ_{Ab}, λ_{Em} and ε for **5** are essentially the same of those measured for **1**. Additionally, the active ester does not seem to affect the excitation dynamics and the ϕ_F of **5** remains close to that of the parent compound.

Photolysis of **5** cleaves the oxazine heterocycle to generate **6** and **7**, as observed for the parent system. Absorption spectra (Figure S11), recorded during the course of the photochemical transformation, reveal the developing absorption of **6** at a λ_{Ab} of 656 nm with a ε of 76.8 mM^{-1} cm^{-1} (***b*** in Figure S9). These values differ slightly from those of the parent system, because the photoinduced disconnection of the oxazine heterocycle brings the active ester in conjugation with the BODIPY chromophore. Analysis of the temporal absorbance evolution, during photolysis, indicates the quantum yield for the photochemical transformation to be 0.01. Selective excitation of the photochemical product within the developing absorption generates fluorescence (***d*** in Figure S9) at a λ_{Em} of 669 nm and a ϕ_F of 0.40. These values are remarkably similar to those of the parent system. Thus, our photoactivatable BODIPY retains its photochemical and photophysical properties almost unaffected even after substitution with an active ester.

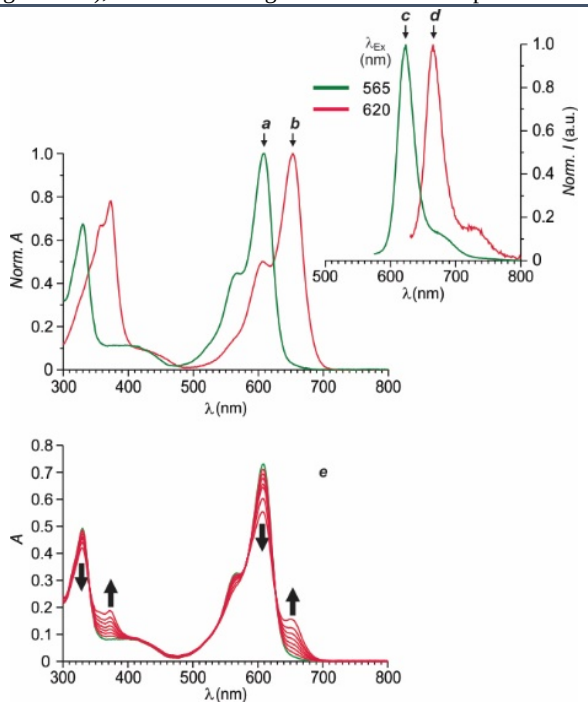

Figure 2. Normalized absorption and emission spectra of **1** (***a*** and ***c***) and **2** (***b*** and ***d***) in THF. Absorption spectra (***e***) of a THF solution of **1** (10 μM) recorded before and during irradiation (350 nm, 4.2 mW cm^{-2}, 10 min).

The excellent photophysical properties of our photoactivatable fluorophores permit the characterization of their fluorescence at the single-molecule level. Specifically, the photoactivation of **1** can be monitored within a poly(methyl methacrylate) (PMMA) film using a spectroscopic photon localization microscopy (SPLM) setup, which simultaneously collects spatial and spectral information of single-molecule emission events.[30] Illumination of the doped polymer film at a λ_{Ex} of 642 nm shows minimal fluorescence, because the absorbance of **1** is negligible at this wavelength. After activation at a λ_{Ac} of 405 nm, intense fluorescence is detected at the single-molecule level, under the same 642-nm excitation conditions, as a result of the photoinduced formation of **2**. The averaged single-molecule emission spectrum (***a*** in Figure 3) of 8,971 photoactivated events shows a λ_{Em} of 670 nm, confirming that photoactivation can be replicated within the PMMA matrix at the single-molecule level.

The high brightness of **2** permits the observation of the spectral evolution for a single photoactivation process. Upon photoactivation, a single molecule of **2** can be detected unambiguously and its emission spectrum can be monitored until photobleaching (***b*** in Figure 3). The emission intensity and spectrum fluctuate over the entire acquisition time (***c*** in Figure 3). The standard deviation (σ_{Sc}) for the weighted spectral center wavelength[31] (λ_{Sc}) distribution is 1.74 nm. The high resistance of **2** to photodegradation requires an illumination power of 500 W cm^{-2} at 642 nm to ensure photobleaching in tens of milliseconds and enable the high-throughput detection of multiple photoactivation events at the single-molecule level. The emission intensities and spectra of 8,971 photoactivated events reveal larger

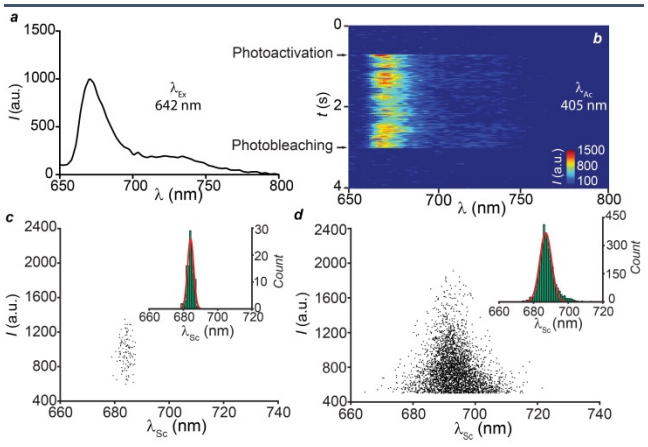

Figure 3. Emission spectrum (***a***), averaged over 8,971 single molecules, of a photoactivated PMMA film doped with **1** and spectral evolution (***b***) of a single molecule after photoactivation. Plots (***c*** and ***d***) of the emission intensity against the spectral centroid and spectral centroid distributions (insets) with Gaussian fitting (red lines), showing the spectral fluctuation of a single molecule (***c***) and the spectral heterogeneity (***d***) among all events.

variations than a single one (***d*** in Figure 4). The value of λ_{Sc} fluctuates for as much as 60 nm with a σ_{Sc} of 5.0 nm. Presumably, environmental inhomogeneities across different regions of the substrate are responsible for the large spectral heterogeneity, compared to the spectral fluctuations of a single molecule. Indeed, differences in the local environment around individual emitters are known to affect their spectral output.[31]

Images, acquired with a confocal laser-scanning microscope (CLSM), of COS-7 cells incubated with **1** (***a*** in Figure S12) or **5** (***a***, ***d*** and ***g*** in Figure 4) show intense intracellular fluorescence upon excitation at a λ_{Ex} of 561 nm. Co-incubation with lysosomal (***b*** in Figures 5 and S12), mitochondrial (***e*** in Figure 4) or nuclear (***h*** in Figure 4) stains reveals exclusive co-localization in the lysosomes (***c*** in Figures 4 and S12) with a Pearson's coefficient of 0.98. No mitochondrial (***f*** in Figure 4) and nuclear (***i*** in Figure 4) co-localizations are detected.

The internalized probes (**1** or **5**) can be photoactivated in the intracellular environment of live COS-7 cells to track the bright photochemical products (**2** or **6**) at the single-molecule level. Interestingly, **2** appears to diffuse for hundreds of nanometers intracellularly (Figure S13), while **6** remains localized at the photoactivated site for prolonged times (Figure S14). Indeed, the active ester of **5** is designed to anchor the internalized photoactivatable fluorophores to the abundant primary amines of the intracellular proteins. In fact, this particular functional group is routinely employed to immobilize synthetic probes intracellularly.[32]

The suppression of intracellular diffusion and high brightness engineered into our photoactivatable fluorophores enable the reconstruction of super-resolution images of live cells with optimal localization performance. The lysosomal localization of the photoactivatable probes, evident from the CLSM images of COS-7 cells incubated with **5**, can be exploited to visualize these intracellular compartments with spatial resolution at the nanometer level on the basis of PALM. Furthermore, the photochemical mechanism for fluorescence activation designed into our molecules permits the acquisition of PALM images in the cell-growth medium without the addition of oxygen scavengers or antioxidants.[16] Once again, **5** switches to **6**, under mild 405-nm illumination, and the latter can be selectively excited with a λ_{Ex} of 642 nm. Within tens of milliseconds, the photoactivated fluorophores photobleach irreversibly and cannot produce further fluorescence. As a result, the reiterative photoactivation and photobleaching of sub-populations of **5** and **6** respectively enable the reconstruction of sub-diffraction images of the labeled lysosomes with localization precision at the nanometer level. Specifically, the intensity trajectory (***d*** in Figure 5) of the photoactivation/photobleaching process from a 7 × 7 pixel area shows distinct intensity spikes over the entire acquisition time. The reconstructed images (***a***–***c*** in Figure 5) reveals individual lysosomes that would otherwise be impossible to resolve with conventional epi-fluorescence microscopy. The line profiles of the green- and blue-highlighted regions indicate the size of individual lysosomes to be *ca.* 80 nm (***e*** in Figure 5), consistently with literature values.[33] The localization precision is *ca.* 15 nm with a mean photon count of *ca.* 2,000 (***f*** and ***g*** in Figure 5).

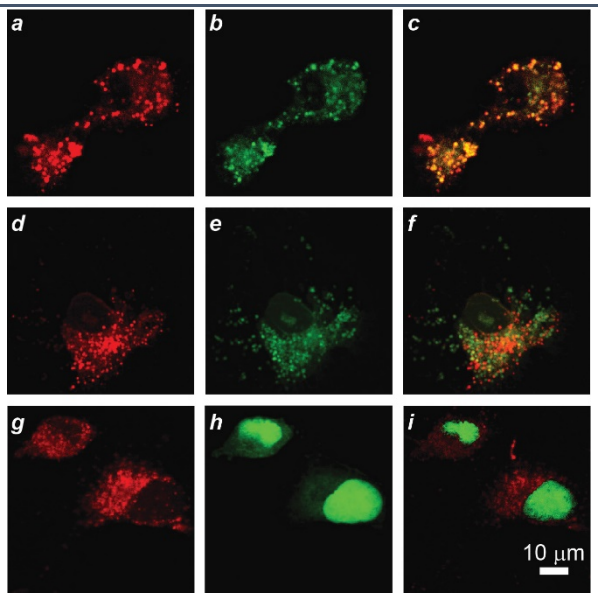

Figure 4. CLSM images of live COS-7 cells incubated with **5** (***a***, ***d*** and ***g***) and lysosomal (***b***), mitochondrial (***e***) or nuclear (***h***) stains together with the corresponding overlays (***c***, ***f*** and ***i***).

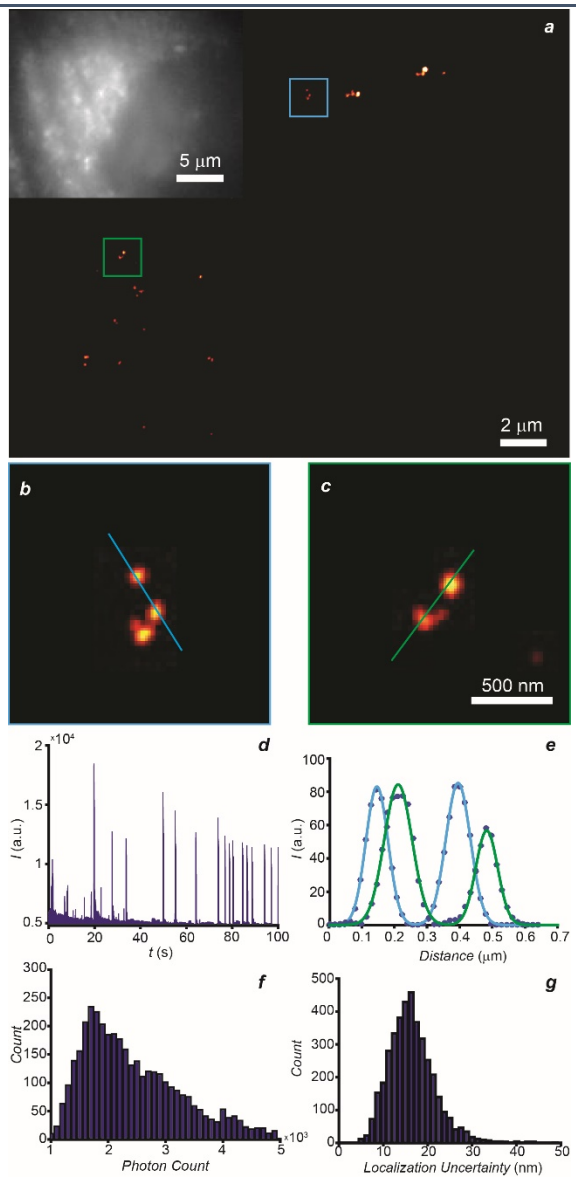

Figure 5. PALM (***a***) and epi-fluorescence (inset) images of a COS-7 cell labeled with **5**. Magnifications (***b*** and ***c***) of the highlighted regions. Representative single-molecule blinking trajectory (***d***), recorded within a 7 × 7 pixel area in the same sample after photoactivation. Line measurements (***e***) with Gaussian fitting of individual lysosomes in ***b*** and ***c***. Photon count (***f***) and localization uncertainty (***g***) parameters of the single-molecule photoactivation events.

In summary, our structural design ensures photoactivation of bright far-red fluorescence with infinite contrast in the lysosomal compartments of live cells together with negligible intracellular diffusion. Such a combination of properties allows the unprecedented visualization of labeled organelles in live cells with localization precision of 15 nm. Thus, our photoactivatable fluorophores can evolve into invaluable analytical tools for single-molecule tracking and localization microscopy within intracellular components of live cells.

ASSOCIATED CONTENT

Supporting Information

The Supporting Information is available free of charge on the ACS Publications website at DOI: #.
Experimental procedures; spectroscopic data; fluorescence images

AUTHOR INFORMATION

Corresponding Author

*hfzhang@northwestern.edu
*fraymo@miami.edu

Notes

H.F.Z. and C.S. have financial interests in Opticent Health, which did not fund this work. All remaining authors declare no competing financial interests.

ACKNOWLEDGMENT

The National Science Foundation (CHE-1505885, CBET-1706642 and EEC-1530734), National Institute of Health (R01EY026078 and R01EY029121) and Northwestern University Innovative Initiative Incubator (I3) Award are acknowledged for financial support.

REFERENCES

(1) Betzig, E. *Angew. Chem. Int. Ed.* **2015**, *54*, 8034–8053.
(2) Hell, S. W. *Angew. Chem. Int. Ed.* **2015**, *54*, 8054–8066.
(3) Moerner, W. E. *Angew. Chem. Int. Ed.* **2015**, *54*, 8067–8093.
(4) Raymo, F. M. *Phys. Chem. Chem. Phys.* **2013**, *15*, 14840–14850.
(5) van de Linde, S.; Sauer, M. *Chem. Soc. Rev.* **2014**, *43*, 1076–1087.
(6) Gorka, A. P.; Nani, R. R.; Schnermann, M. J. *Org. Biomol. Chem.* **2015**, *13*, 7584–7598.
(7) Lavis, L. D. *Annu. Rev. Biochem.* **2017**, *86*, 825–843.
(8) Loudet, A.; Burgess, K. *Chem. Rev.* **2007**, *107*, 4891−4932.
(9) Ziessel, R.; Ulrich, G.; Harriman, A. *New J. Chem.* **2007**, *31*, 496–501.
(10) Ulrich, G.; Ziessel, R.; Harriman, A. *Angew. Chem. Int. Ed.* **2008**, *47*, 1184–1201.
(11) Benstead, M.; Mehl, G. H.; Boyle, R. W. *Tetrahedron* **2011**, *67*, 3573–3601.
(12) Boens, N.; Leen, V.; Dehaen, W. *Chem. Soc. Rev.* **2012**, *41*, 1130–1172.
(13) Kamkaew, A.; Lim, S. H.; Lee, H. B.; Kiew, L. V.; Chung, L. Y.; Burgess, K. *Chem. Soc. Rev.* **2013**, *42*, 77–88.
(14) Lu, H.; Mack, J.; Yang, Y.; Shen, Z. *Chem. Soc. Rev.* **2014**, *43*, 4778–4823.
(15) Ni, Y.; Wu, J. *Org. Biomol. Chem.* **2014**, *12*, 3774–3791.
(16) Shim, S.-H.; Xia, C.; Zhong, G.; Babcock, H. P.; Vaughan, J. C.; Huang, B.; Wang, X.; Xu, C.; Bi, G.-Q.; Zhuang, X. *Proc. Natl. Acad. Sci. USA* **2012**, *109*, 13978–13983.
(17) Wijesooriya, C. S.; Peterson, J. A.; Shrestha, P.; Gehrmann, E. J.; Winter, A. H.; Smith, E. *Angew. Chem. Int. Ed.* **2018**, *57*, 10.1002/anie.201805827.
(18) Kobayashi, T.; Komatsu, T.; Kamiya, M.; Campos, C.; González-Gaitán, M.; Terai, T.; Hanaoka, K.; Nagano, T.; Urano, Y. *J. Am. Chem. Soc.* **2012**, *134*, 11153−11160.
(19) Shaban Ragab, S.; Swaminathan, S.; Baker, J. D.; Raymo, F. M. *Phys. Chem. Chem. Phys.* **2013**, *15*, 14851–14855.
(20) Ragab, S.; Swaminathan, S.; Deniz, E.; Captain, B.; Raymo, F. M. *Org. Lett.* **2013**, *15*, 3153–3157.
(21) Amamoto, T.; Hirata, T.; Takahashi, H.; Kamiya, M.; Urano, Y.; Santa, T.; Kato, M. *J. Mater. Chem. B* **2015**, *3*, 7427–7433.
(22) Goswami, P. P.; Syed, A.; Beck, C. L.; Albright, T. R.; Mahoney, K. M.; Unash, R.; Smith, E. A.; Winter, A. H. *J. Am. Chem. Soc.* **2015**, *137*, 3783−3786.
(23) Hess, S. T.; Girirajan, T. P. K.; Mason, M. D. *Biophys. J.* **2006**, *91*, 4258–4272.
(24) Betzig, E.; Patterson, G. H.; Sougrat, R.; Lindwasser, O. W.; Olenych, S.; Bonifacino, J. S.; Davidson, M. W.; Lippincott-Schwartz, J.; Hess, H. F. *Science* **2006**, *313*, 1642–1645.
(25) Zhang, Y.; Swaminathan, S.; Tang, S.; Garcia-Amorós, J.; Boulina, M.; Captain, B.; Baker, J. D.; Raymo, F. M. *J. Am. Chem. Soc.* **2015**, *137*, 4709–4719.
(26) Zhang, Y.; Tang, S.; Sansalone, L.; Baker, J. D.; Raymo, F. M. *Chem. Eur. J.* **2016**, *22*, 15027–15034.
(27) Liu, X.; Zhang, Y.; Baker, J. D.; Raymo, F. M. *J. Mater. Chem. C* **2017**, *5*, 12714–12719.
(28) Sansalone, L.; Tang, S.; Garcia-Amoros, J.; Zhang, Y.; Nonell, S.; Baker, J. D.; Captain, B.; Raymo, F. M. *ACS Sens.* **2018**, *3*, 1347–1353.
(29) Tang, S.; Zhang, Y.; Dhakal, P.; Ravelo, L.; Anderson, C. L.; Collins, K. M.; Raymo, F. M. *J. Am. Chem. Soc.* **2018**, *140*, 4485−4488.
(30) Dong, B.; Almassalha, L.; Urban, B. E.; Nguyen, T.-Q.; Khuon, S.; Chew, T.-L.; Backman, V.; Sun, C.; Zhang, H. F. *Nat. Commun.* **2016**, *7*, 12290-1–8.
(31) Lu, H. P.; Xie, X. S. *Nature* **1997**, *385*, 143–146.
(32) Johnson, I. D. (Ed) *Molecular Probes Handbook: A Guide to Fluorescent Probes and Labeling Technologies*; Life Technologies Corporation: Grand Island: 2010.
(33) He, H.; Ye, Z.; Zheng, Y.; Xu, X.; Guo, C.; Xiao, Y.; Yang, W.; Qian, X.; Yang, Y. *Chem. Commun.* **2018**, *54*, 2842–2845.

Graphical Abstract